Electrochemical evidences of morphological transformation in ordered mesoporous titanium oxide thin films†

Mathieu Etienne,*[a] David Grosso,[b] Cédric Boissière,[b] Clément Sanchez[b] and Alain Walcarius[a]

Received (in Cambridge, UK) 9th June 2005, Accepted 22nd July 2005
First published as an Advance Article on the web 17th August 2005
DOI: 10.1039/b508093b

We provide the first electrochemical evidence of permeability changes in continuous mesoporous TiO_2 thin film electrodes induced by nanocrystallisation.

Mesoporous TiO_2 thin film are promising material in a wide range of technological applications such as electrochromism,[1] photovoltaic electrodes,[2] photocatalysis[3] and electrochemical (bio)sensors.[4] Up to now, most electrochemical studies involving mesoporous titanium oxide thin films have been performed with electrodes prepared by deposition and sintering of TiO_2 nanoparticles, leading to aggregates of particles (eventually with a binder) on the electrode surface rather than a continuous inorganic single phase exhibiting regular and periodic porosity.[5] Continuous mesoporous TiO_2 thin film electrodes remain rare.[6] When considering the electrochemical applications of porous thin films, particular attention has to be given to mass transport issues into the film (*i.e.*, from the solution to the electrode surface). From this point of view, earlier works on the electrochemistry of mesoporous silica thin films deposited on solid electrode surfaces have shown that, despite the favourable mass transport expected from the ordered mesoporous architecture,[13] strong diffusional limitations might be observed due to unfavourable orientation of the mesopores parallel to the electrode surface,[14] or to the formation of a microporous barrier between the electrode and the mesoporous layer.[15]

The recent extension of Evaporation Induced Self Assembly (EISA), initially introduced for the preparation of mesoporous silica thin film,[7,8] to mesoporous transition metal oxide[8,9] has permitted the elaboration of highly ordered mesoporous TiO_2 thin films.[10–12] The preparation involves sol–gel deposition of an amorphous TiO_2 gel in the presence of triblock copolymers under controlled humidity conditions, aging and final thermal crystallisation. Careful studies of the process have shown that aging and crystallisation of the amorphous TiO_2 to nanocrystalline anatase involved a simultaneous dramatic reorganisation of the mesoporous architecture. As-prepared films exhibit body centred cubic mesostructure (space group *Im*3*m*) with organised domains preferentially aligned with their [110] direction normal to the interface. After consolidation of the inorganic mesostructure at 100 °C for 30 min and removal of the surfactant at 300 °C for 20 min, the unidirectional shrinkage induced by the drying and thermal treatment applies perpendicularly to the surface and provokes the transformation of the initial mesostructure into a contracted cubic structure having orthorhombic symmetry (Fig. 1A, TiO_2-gel).[11] Upon crystallisation at 500 °C for 10 min, this latter structure is turned into a grid-like structure of bi-directional mesoporous parallel networks standing perpendicular to the substrate surface (Fig. 1B and C, TiO_2-anatase).[12] Electrochemistry was applied here to point out this structural change and to evaluate its consequence on mass transfer into the mesoporous thin film deposited on fluorine-doped tin oxide (FTO) electrodes.‡

Due to the semi-conducting and redox properties of TiO_2, a prerequisite for any electrochemical measurement performed with TiO_2 modified electrodes is to determine the potential window in which the electrode response to solution-phase redox probes is not affected by the TiO_2 thin film. It has been observed that FTO electrodes modified by continuous mesoporous TiO_2 thin films (gel and anatase) displayed potential windows with limits around −0.5 V and +1.7 V, respectively in the cathodic and anodic regions (Figure A and related discussion in ESI†). These limits are compatible with the redox probes used in this study ($Ru(bpy)_3^{2+}$, $Fe(CN)_6^{3-}$, I^-, Cu^{2+}, Meldola's blue and Au(IV)).

Fig. 2 illustrates the effect of the TiO_2 film on the FTO electrode (after template removal and respectively before and after crystallisation at 500 °C) on the electrochemical response obtained in 1 mM $Ru(bpy)_3^{2+}$ solution (phosphate buffer, pH 6.8). On Bare FTO (curve "a"), the CV signal is characteristic of a quasi-reversible system (ΔE = 0.12 V; ½ (E^{ox} + E^{red}) = 1.07 V) with peak currents of 84 μA (I^{ox} = I^{red}). Similar behaviour was observed at pH 4.1 except that the system was even less reversible (ΔE = 0.17 V). Once the FTO electrode was covered with a mesoporous titania thin film displaying a contracted cubic mesophase after surfactant removal (TiO_2-gel), the voltammetric curve recorded in the same conditions was completely flat (curve "b"). The absence of signal demonstrates unambiguously

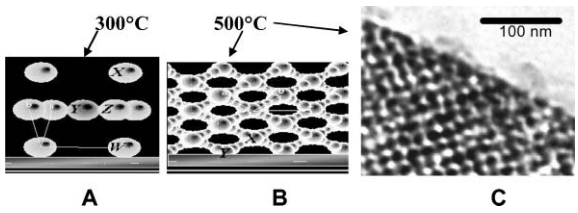

Fig. 1 Illustration of the mesoporous TiO_2 architecture obtained at (A) 300 °C (closed contracted bcc) and (B) 500 °C (open grid-like). TEM picture of the open grid like structure stabilised at 500 °C (C).

[a]*Laboratoire de Chimie Physique et Microbiologie pour l'Environnement, UMR 7564, CNRS-Université, H. Poincaré Nancy I. 405, rue de Vandoeuvre, F-54600 Villers-lès-Nancy, France. E-mail: etienne@lcpme.cnrs-nancy.fr; Fax: +33 3 83 27 54 44*
[b]*Laboratoire de Chimie de la Matière Condensée, UMR 7574, CNRS-Université, Pierre et Marie Curie.4, place Jussieu, 75252 Paris Cedex 05*
† Electronic Supplementary Information (ESI) available: Additional results and discussion. See http://dx.doi.org/10.1039/b508093b

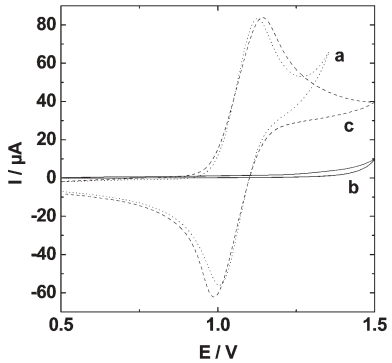

Fig. 2 Cyclic voltammetric curves recorded in 1 mM $Ru(bpy)_3^{2+}$ (in 0.1 M phosphate buffer solution at pH 6.8) using (a) bare FTO, (b) TiO_2-gel–FTO, and (c) TiO_2-anatase–FTO electrodes; film thickness of about 160 nm (b, c); scan rate: 50 mV s^{-1}.

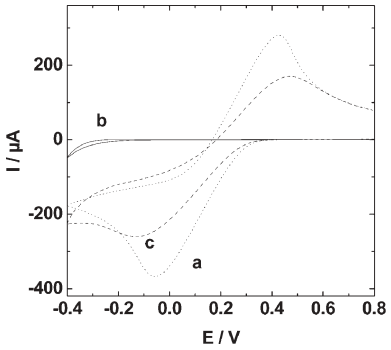

Fig. 3 Cyclic voltammetric curves recorded in 5 mM $Fe(CN)_6^{3-}$ (in 0.05 M hydrogen phthalate solution at pH 4.1) using (a) bare FTO, (b) TiO_2-gel–FTO, and (c) TiO_2-anatase–FTO electrodes; film thickness of about 125 nm (b, c); scan rate: 50 mV s^{-1}.

that the contracted cubic structure of the mesoporous thin film deposited on the electrode surface acts as a physical barrier for the solution-phase $Ru(bpy)_3^{2+}$ species. This also confirms the homogeneous character of the titania film and the absence of defects on the nanometre scale. The situation was completely different, and far more advantageous, after crystallisation of the mesoporous TiO_2 film at 500 °C (for 10 min), giving rise to an electrochemical response (curve "c") very close to that observed on bare FTO. Peak heights were identical while the anodic-to-cathodic peak potential difference was characterised by a slightly higher overpotential (ΔE = 0.15 V) in comparison to the bare electrode, which could be due to the small difference in resistance between the two electrochemical cells (160 Ω with FTO and 250 Ω with TiO_2-anatase–FTO, as determined by the ohmic drop compensation technique). No distinguishable effect of film thickness was observed in the 90–160 nm range. The above results clearly point out the overwhelming interest of the structural variation during the thermal treatment at high temperature to enhance the film electrode performance. As the film porosity (pore diameter estimated at 7 nm)[12] was large in comparison to the size of the probe (about 1.1 nm for $Ru(bpy)_3^{2+}$)[16] no significant diffusional limitations were observed. As its thickness was rather low (in the 100 nm range) in comparison to the thickness of the diffusion layer (*i.e.*, 100–200 μm in the time scale of the CV experiments), this resulted in peak currents of the same magnitude as those obtained at the bare electrode. Similar results have been obtained with Meldola's blue (MB). However, it seems that the planar geometry of MB enables its entrapment in the contracted cubic mesoporous structure of the thin film treated at 300 °C, giving rise to a non negligible electrochemical response, in contrast to the more bulky $Ru(bpy)_3^{2+}$ which is not likely to penetrate in such a confined environment and, therefore, is electrochemically silent (section B in ESI†).

In order to point out any eventual charge effect, cyclic voltammetry experiments have been also performed using $Fe(CN)_6^{3-}$ (5 mM at pH 4.1) as the redox probe. Typical results have been gathered in Fig.. 3 where curve "a" reports the CV response recorded on the bare FTO electrode; as shown, the $Fe(CN)_6^{3-/4-}$ system (ΔE = 0.48 V) is less reversible than the $Ru(bpy)_3^{2+/3+}$ couple (ΔE = 0.12 V) and exhibited peak currents of about 370 μA. The presence of the mesoporous titania thin film treated at 300 °C resulted in the same blocking effect (curve "b") as that observed previously for $Ru(bpy)_3^{2+}$ species, for the same reasons of physical barrier. More intriguing was the behaviour of $Fe(CN)_6^{3-}$ at the pore-rich grid-like layers intercalated perpendicularly to the electrode surface (curve "c"), as obtained after treatment at 500 °C, which resulted in significant decrease in peak currents (by 30%) and larger overpotentials (ΔE = 0.58 V) in comparison to the bare electrode. This indicates a possible lowering of the electron transfer rates, probably not associated with any resistance to mass transport across the film, because the size of $Fe(CN)_6^{3-}$ (0.7 nm) is smaller than that of $Ru(bpy)_3^{2+}$ (1.1 nm).

When performing similar CV measurements at higher pH in phosphate buffer (pH 6.8), $Fe(CN)_6^{3-}$ reduction became even more difficult (E^{red} = −0.40 V instead of −0.10 V at pH 4.1). Two factors seem to limit the redox processes of the $Fe(CN)_6^{3-/4-}$ system. Firstly, the large overpotentials are indicative of restricted electron transfer kinetics and, secondly, resistance to mass transport seems to increase when increasing the film thickness (~25% current lost from 90 to 125 nm). This latter, which was not observed in phthalate medium at pH 4.1, can be explained by the existence of negative charges on the anatase surface at pH 6.8 (point of zero charge ≈ 5.5),[17] which are even more numerous in phosphate medium due to the well-known adsorption of phosphate moieties on titanium oxides.[18] The limitations observed for the $Fe(CN)_6^{3-}$ probe in CV would thus be explained by electrostatic repulsion. This was further confirmed by using another negatively-charged redox species, I^-, for which no difference in the CV peak heights for the bare FTO and the TiO_2-anatase–FTO electrodes was observed at pH 4.1, whereas the TiO_2-anatase–FTO electrode was characterised by a significant decrease in sensitivity in phosphate buffer at pH 6.8.

The TiO_2-anatase–FTO electrode is also attractive support for the growth of metal nanostructures. Fig.. 4 illustrates some results obtained for the electrodeposition of gold applying a constant potential electrolysis from a commercially available electroplating solution (Aurocor®). This potential (−0.65 V *vs.* Ag/AgCl) was chosen as the best compromise to enable metallic gold deposition and to prevent reduction of the TiO_2 material as much as possible. Curve "a" shows the chronoamperogram obtained with the thinner film treated at only 300 °C, which looks like a capacitive decay with negligible faradaic contribution (no significant electrodeposition, as confirmed by no visual detection of any gold deposit (picture "1A" in the inset of Fig. 4), in agreement with the above

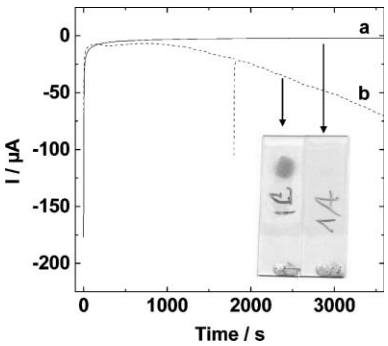

Fig. 4 Chronoamperometric curves recorded by applying a constant potential of −0.65 V (*vs.* Ag/AgCl) in Aurocor® solution at (a) TiO_2-gel–FTO and (b) TiO_2-anatase–FTO electrodes; film thickness of about 90 nm; curve (b) has been obtained in two steps, by recording the current signal for 30 min, interrupting the application of potential for 10 min and measuring again the current response on the same surface for the next 30 min. Inset: visual aspect of the two modified FTO electrodes after one hour electrodeposition: "1A" refers to the TiO_2-gel–FTO sample and "1C" to the TiO_2-anatase–FTO electrode.

results). Using the film electrode treated at 500 °C (TiO_2-anatase–FTO) resulted in a continuous increase of cathodic currents after the starting capacitive decay (Fig. 4, curve "b"). This regular increase is due to the progressive enlargement of the effective electrode surface area due to the formation of increasing amounts of metallic gold nanostructures. This increase was not affected by imposing a delay during the electrodeposition process: stopping the experiment for some minutes (*i.e.*, after 30 min deposition) did not result in any break in the current response profile except, of course, the new capacitive decay due to applying again the potential step. After one hour of electrodeposition, a gold disk is clearly visible on the thin film treated at 500 °C (picture "1C" in the inset of Fig. 4), corresponding to the electrode area in contact with the gold plating solution. The gold deposits cover the whole surface of the exposed sample, demonstrating the homogeneous character of the mesoporous TiO_2-anatase layer. From integration of the chronoamperometric curve (*i.e.*, 0.10 C), one can estimate the thickness of the gold deposit at about 150 nm, corresponding to pore filling within the 90 nm-thick TiO_2 layer overcoated with a ~60 nm-thick pure gold deposit. Copper electrodeposition is also discussed in ESI (section C†).

In summary, we provide the first demonstration of permeability changes in mesoporous thin film TiO_2 electrodes induced by nanocrystallisation. Electrochemistry has allowed demonstration of the huge impact of crystallisation of ordered mesoporous TiO_2 thin films on mass transport and charge transfer processes at this new generation of thin film electrodes. This has been shown in this work *via* the nearly complete suppression of the voltammetric signals on the TiO_2-gel–FTO electrode (*i.e.*, treated at 300 °C) while the TiO_2-anatase–FTO electrode (*i.e.*, treated at 500 °C) gave rise to well-defined CV responses with peak heights up to those recorded at the bare FTO electrode. The TiO_2-anatase–FTO electrode was also found to be a good support for metal electrodeposition. The fast mass transport processes observed in ordered mesoporous TiO_2-anatase thin film deposited on solid electrodes would contribute to opening new opportunities for improving the performance of such integrated electrochemical systems with respect to applications in various fields including electroanalysis, electrocatalysis, biosensors, electrochromism, or photovoltaic devices.

Notes and references

‡ Thin hybrid meso-organised TiO_2 films were prepared as previously reported:[10–12] FTO substrates were withdrawn from a solution containing 1 $TiCl_4$; 10 H_20, 40 EtOH, and 0.005 $HO(CH_2CH_2O)_{106}-(CH_2-CH(CH_3)O)_{70}(CH_2CH_2O)_{106}H$ (Pluronic F127) (molar ratio) with the following humidity sequence of 10% during evaporation and 60% during the following 24 hours of aging. Film thickness has been adjusted by varying the dip-coating speed from 1 to 4 mm s^{-1}. Film thicknesses were deduced from Ellipsometry analysis using a Woollam VASE M-2000U apparatus. All electrochemical experiments were performed with a PGSTAT12 Autolab potentiostat controlled by the GPES electrochemical software (Eco Chemie), in a conventional three-electrode cell. The working electrode was the FTO modified electrode. The surface of the electrode was delimited by an O-ring (1 mm thick and 9 mm inner diameter) on which was placed a Teflon reservoir containing the solution. A Pt wire served as the counter electrode and an Ag/AgCl electrode (Metrohm) was used as the reference.

1 For example: (*a*) N. N. Dinh, N. Th. T. Oanh, P. D. Long, M. C. Bernard and A. Hugot-Le Goff, *Thin Solid Films*, 2003, **423**, 70; (*b*) S. Y. Choi, M. Mamak, N. Coombs, N. Chopra and G. A. Ozin, *Nano Lett.*, 2004, **4**, 1231.
2 For example: (*a*) A. Hagfeldt and M. Grätzel, *Acc. Chem. Res.*, 2000, **33**, 269; (*b*) H. Tokuhisa and P. T. Hammond, *Adv. Funct. Mater.*, 2003, **13**, 831.
3 For example: A. Heller, *Acc. Chem. Res.*, 1995, **28**, 503.
4 For example: (*a*) E. Topoglidis, A. E. G. Cass, B. O'Regan and J. R. Durrant, *J. Electroanal. Chem.*, 2001, **517**, 20; (*b*) K.-R. Meier and M. Grätzel, *ChemPhysChem*, 2002, 371; (*c*) S. Cosnier, C. Gondran, M. Grätzel and N. Vlachopoulos, *Electroanalysis*, 1997, **9**, 1387.
5 B. O'Regan and M. Grätzel, *Nature*, 1991, **353**, 737.
6 L. Kavan, J. Rathousky, M. Grätzel, V. Shklover and A. Zukal, *Microporous Mesoporous Mater.*, 2001, **44–45**, 653.
7 (*a*) Y. Lu, R. Ganguli, C. A. Drewien, M. T. Anderson, C. J. Brinker, W. Gong, Y. Guo, H. Soyez, B. Dunn, M. H. Huang and J. I. Zink, *Nature*, 1997, **389**, 364; (*b*) C. J. Brinker, Y. Lu, A. Sellinger and H. Fan, *Adv. Mater.*, 1999, **11**, 579.
8 D. Grosso, F. Cagnol, G. J. A. A. Soler-Illia, E. L. Crepaldi, H. Amenitsch, A. Brunet-Bruneau, A. Bourgeois and C. Sanchez, *Adv. Funct. Mater.*, 2004, **14**, 309.
9 F. Schüth, *Chem. Mater.*, 2001, **13**, 3184.
10 D. Grosso, G. J. A. A. Soler-Illia, F. Babonneau, C. Sanchez, P.-A. Albouy, A. Brunet-Bruneau and A. R. Balkenende, *Adv. Mater.*, 2001, **13**, 1085.
11 E. L. Crepaldi, G. J. A. A. Soler-Illia, D. Grosso, F. Cagnol, F. Ribot and C. Sanchez, *J. Am. Chem. Soc.*, 2003, **125**, 9770.
12 D. Grosso, G. J. A. A. Soler-Illia, E. L. Crepaldi, F. Cagnol, C. Sinturel, A. Bourgeois, A. Brunet-Bruneau, H. Amenitsch, P. A. Albouy and C. Sanchez, *Chem. Mater.*, 2003, **15**, 4562.
13 A. Walcarius, M. Etienne and B. Lebeau, *Chem. Mater.*, 2003, **15**, 2161.
14 C. Song and G. Villemure, *Microporous Mesoporous Mater.*, 2001, **44–45**, 679.
15 M. Etienne and A. Walcarius, submitted.
16 S. Bélanger, J. T. Hupp, C. L. Stern, R. V. Slone, D. F. Watson and T. G. Carrell, *J. Am. Chem. Soc.*, 1999, **121**, 557.
17 G. A. Parks, *Chem. Rev.*, 1965, **65**, 177.
18 P. C. Angelomé, S. Aldabe-Bilmes, M. E. Calvo, E. L. Crepaldi, D. Grosso, C. Sanchez and G. J. A. A. Soler-Illia, *New J. Chem.*, 2005, **29**, 59.